Research Square

Preprints are preliminary reports that have not undergone peer review.
They should not be considered conclusive, used to inform clinical practice,
or referenced by the media as validated information.

Similarity Theory of Epidemic Waves: From Universal Dynamics to Peak Hospitalization

Felix Mairanowski

felma39@yahoo.de

SmairGmbH https://orcid.org/0000-0002-3678-0198

Below Denis

Alexianer Krankenhaus Hedwighöhe https://orcid.org/0009-0004-3282-8387

Research Article

Keywords: similarity theory, pandemic response, epidemic management, hospital capacity, decision support, scale invariance

Posted Date: November 16th, 2026

DOI: https://doi.org/10.21203/rs.3.rs-11717235/v1

License: This work is licensed under a Creative Commons Attribution 4.0 International License.
Read Full License

Additional Declarations: The authors declare no competing interests.

Similarity Theory of Epidemic Waves: From Universal Dynamics to Peak Hospitalization

Authors: Denis Below [1], Felix Mairanowski [2]

Affiliations:

[^1] Alexianer Krankenhaus Hedwigshöhe, Berlin, Germany, orcid.org/0009-0004-3282-8387

[^2] Smair Tech. GmbH, Berlin, Germany, orcid.org/0000-0002-3678-0198

Corresponding author: Denis Below . Email Address: denisbelow@hotmail.de

Keywords: similarity theory, pandemic response, epidemic management, hospital capacity, decision support, scale invariance

Abstract

During infectious disease outbreaks, healthcare managers require rapid tools to project peak hospital workloads without heavy computer simulations. This paper introduces a simple mathematical method that treats epidemic waves as natural, self-limiting events. By converting absolute case numbers into relative percentages, our framework completely removes structural differences associated with regional geography and population size. We demonstrate that the universal shape of a wave is independently governed by only two driving forces: the biological spreading power of the virus and the behavioural contact reduction rate of the population. Under this transformation, complex disease trajectories from highly diverse regions flatten and merge symmetrically into a single, predictable pattern.

Combining public behaviour metrics with hospital discharge rates yields a straightforward formula to calculate peak bed demand. The results prove a major operational asymmetry: public contact reduction provides significantly higher immediate protection for hospitals during acute growth phases than accelerating vaccine distribution. This approach allows health authorities to monitor a small pilot group and scale the findings to project national capacity needs in real time.

Introduction

Epidemic waves can differ greatly in size and timing, yet their large-scale growth and decline may follow similar patterns. Identifying such patterns could make it possible to compare epidemic waves across populations without reproducing every local biological, demographic, and behavioural detail.

Most established epidemic models describe transmission using compartmental systems such as SIR and SEIR, often supplemented by demographic, clinical, and behavioural variables [1,2]. These models are powerful and flexible, but their complexity can make it difficult to identify simple relationships between the overall dynamics of an epidemic wave and the resulting demand for healthcare. A complementary approach is to describe epidemic transmission at the macroscopic level, using effective parameters that represent the collective behaviour of a population.

Our earlier work introduced a macroscopic differential model for epidemic-wave dynamics and applied it to COVID-19 data [4]. That formulation provided the basic equations used in the present study. Here, we develop the model further by applying similarity theory and dimensional analysis to identify the dimensionless parameters governing its large-scale behaviour. This allows epidemic trajectories from populations with different sizes and transmission conditions to be expressed within a common reduced representation.

The idea is analogous, at a methodological level, to approaches used in macroscopic science and engineering: the detailed behaviour of a complex system can sometimes be described through a small number of effective parameters without resolving every microscopic interaction. In the present formulation, the effective transmission coefficient k characterizes the macroscopic ability of infection to spread, while the resistance parameter λ represents the aggregate reduction of effective transmission pathways. This resistance may reflect formal interventions, behavioural adaptation, mobility changes, and other population-level responses.

An important practical consequence of similarity is that observations or controlled interventions performed in a smaller, relatively homogeneous territory may provide information about epidemic dynamics at a larger geographic scale, provided that the relevant dimensionless parameters and boundary conditions are sufficiently similar. This principle is analogous to the use of scaled models in hydrodynamics, aerodynamics, and thermal engineering, where experiments on smaller physical models can be used to infer the behaviour of larger systems. In epidemiology, therefore, similarity theory may provide a basis for testing interventions at a local scale before considering their application to larger populations.

Similarity theory provides a formal way to determine combinations of dimensional variables that remain relevant when the scale of a system changes [11]. Applied to the present epidemic model, it yields dimensionless groups combining transmission, resistance, vaccination, and

time. If epidemic waves share a common macroscopic structure, trajectories from different populations should converge toward a common reduced trajectory when expressed in these variables.

We first derive this similarity representation for an isolated epidemic wave and examine it using COVID-19 trajectories from different regions. We then extend the formulation to active vaccination and successive epidemic-wave segments.

The principal application of the present study is healthcare demand. Hospital occupancy is treated as a downstream response to the inflow of patients generated by epidemic transmission, with admission and discharge represented by effective clinical parameters

The aim is not to replace detailed epidemiological or numerical models. Rather, we develop a transparent macroscopic framework for comparing epidemic waves and connecting their large-scale dynamics to healthcare demand. The approach separates the common structure of epidemic trajectories from population-specific scales while retaining a direct connection to measurable healthcare burden.

2. Model and similarity parameters

2.1. Model Formulation

The macro-evolutionary dynamics of a self-limiting transmission wave within a closed, non-homogeneous regional population N are governed by the following cascaded differential system: [3]:

$$\frac{dS}{dt} = -\lambda * S - \left(\frac{(\alpha * v)}{(1 - \alpha * v * t)}\right) * S \qquad (1)$$

$$\frac{dI_c}{dt} = k_0 * \frac{(S * I_c)}{N} \qquad (2)$$

Where:

Where S(t) represents the continuous host reservoir of susceptible individuals, $I_c(t)$ is the cumulative number of infected individuals, and N is the total regional population. The parameter k_0 denotes the intrinsic, unmitigated biological transmission rate day^{-1}.

The macroscopic system closure is achieved by introducing the endogenous behavioral adaptation parameter, λ day^{-1}. Rather than treating contact network topologies as static mixing fields, λ quantifies the real-world rate of contact reduction within the population driven by

risk-avoidance public feedback, social distancing, and non-pharmaceutical interventions (NPIs). In the context of mathematical physics, this adaptation functions as a macro-scale volume contraction of the active social network.

The structural group $\frac{(\alpha * v)}{(1 - \alpha * v * t)}$ represents a mass-conserving public health immunization campaign, deploying doses at a linear daily rate v with an effective clinical vaccine efficacy α. For the dimensionless formulation, we define the cumulative infected population fraction as:

$$i(t) = \left(\frac{I_{c(t)}}{N}\right) * 100\%$$

2.2. Model Assumptions and Scope of Validity

The analytical framework and its similarity scaling rely on four foundational simplifications reflecting the macro-scale mechanics of transmission, validated by empirical multi-wave datasets:

(i) Decoupled Transmission and Low-Incidence Limits: Total depletion of the susceptible pool due to infection during an individual wave segment is assumed to remain small compared with its initial effective baseline ($\Delta S << S_0$). Empirically, cumulative incidence during ancestral waves remained below approximately 10% of the regional population [5, 6], providing a practical basis for linearizing the transmission operator around the initial effective susceptible state. Because infection-driven depletion is minor within an individual wave segment, the corresponding infection-dependent feedback can be uncoupled from the macroscopic environmental forcing represented in Equation (1), including behavioural restrictions and mass immunization. This decoupling mathematically isolates susceptible depletion from the effective transmission coefficient within a single wave.

(ii) Rapid Humoral Immunity Decay and Parameter Resetting: Clinical studies report substantial declines in protective neutralizing antibody levels over several months [7]. Such changes reduce the effective protection established during a preceding epidemic regime, particularly when a subsequent lineage exhibits substantial antigenic or immune-escape variations. In the present framework, this transition is represented macroscopically by re-initialization of the effective susceptible pool at the corresponding wave boundary. The framework therefore operates as a piecewise-continuous formulation in which S_0, k_0, and λ are updated at regime boundaries. Where empirical seroprevalence or other immunity data are available, the measured residual protection can be incorporated as a corrective shift in the initial effective susceptible state for the subsequent wave segment. This representation allows

changes in pathogen lineage or population response to be incorporated without carrying a single parameter set across biologically distinct epidemic regimes.

(iii) Macroscopic Aggregation of Recovery Dynamics: Because the primary formulation describes the cumulative infection trajectory rather than active prevalence, the explicit clinical recovery rate γ is not required for the derivation of the infection-scale solution. The effective resistance parameter λ can be inferred from the final empirical plateau through the asymptotic relation given by Equation (10), thereby aggregating the macroscopic processes responsible for epidemic deceleration. When active hospital occupancy is considered, the recovery parameter γ is introduced in the downstream hospital balance and remains fully compatible with the closed-form epidemic solution through the corresponding convolution layer.

(iv) Vaccination Kinematics and Domain of Validity: Vaccine impact is coupled to Equation (1) through the time-dependent depletion function $\frac{(\alpha * v)}{(1 - \alpha * v * t)}$, representing a mass-immunization programme with an effective blocking rate α v. Within this formulation, the effective depletion coefficient increases as the remaining susceptible pool decreases. The admissibility condition α v t < 1 defines the temporal domain in which the vaccination formulation remains finite and physically admissible. The denominator introduces a mathematical singularity at $t_{sing} = \frac{1}{(\alpha * v)}$. For the vaccination rates considered here, αv≈0.003–0.008 day^{-1}. The resulting finite singularity time defines the admissible boundary of each vaccination segment. Since the model is formulated as a piecewise trajectory over finite time intervals, the analytical solution remains well defined provided that $\tau < \tau_{sing}$; thus, the singularity does not constrain the calculations performed within the considered piecewise domains.

2.3. Analytical Solution and Invariant Groups

Direct integration of the decoupled susceptible governing equation (Equation 1) yields an explicit, closed-form analytical solution for the remaining susceptible population trajectory:

$$S(t) = S_0 * e^{-\lambda * t} * (1 - \alpha * v * t) \quad (3)$$

Substituting Equation (3) into the linearized transmission operator (Equation 2) under the baseline scenario of unmitigated growth (α * v = 0) establishes a closed analytical trajectory for the infection scale. By introducing the scaled epidemiological time λ * t and the

normalized infection scaling $\frac{\Delta i(t)}{i_0}$, the cumulative evolutionary profile shifts from absolute scales into invariant coordinates:

$$\Delta i(t) = i_0 * \exp\left[\left(\frac{k}{\lambda}\right) * \left(1 - e^{-\lambda * t}\right)\right] \quad (4)$$

where the constituent operational parameters and the governing dimensionless variables are defined as:

$$\Delta i(t) = i(t) - i_f \quad (5)$$

$$k = \frac{(k_0 * S_0)}{N} \quad (6)$$

Here, i_f represents the cumulative infection fraction legacy inherited from the preceding wave at the temporal boundary where the new lineage emerges, i_0 denotes the initial seed fraction of infected individuals, and k is the effective macroscopic transmission coefficient. To secure a standardized coordinate baseline across structurally divergent regional populations, i_0 is parameterized via the empirical tracking benchmark:

$$i_0 = \left(\frac{100}{N}\right)\% \quad (7)$$

Here, Equation (7) anchors the initial evolutionary impulse as a fixed volumetric fraction relative to the total regional population matrix N. While this rigorous boundary condition tightens the initial conditions and complicates early-stage statistical matching due to reporting delays, its macroscopic robustness is exceptionally high.

Mathematically, Equation (4) takes the exact structural form of the classical Gompertz growth kinetics [8]. Originally formulated by Benjamin Gompertz to describe the exponential acceleration of human mortality dynamics, this asymmetrical double-exponential framework is uniquely adapted here. While the original actuarial formulation models the deterministic decay of biological vital force, its appearance in our macroscopic transmission system reflects the exponential accumulation of social and behavioural resistance λ against the pathogen, which effectively forces the self-limiting deceleration of the epidemic wave.

The time at which the epidemic growth rate reaches its maximum velocity is given by:

$$t_{max} = \frac{\ln(\frac{k}{\lambda})}{\lambda} \quad (8),$$

The value of the maximum daily increase in the cumulative infected fraction (the peak incidence velocity j_{max} is derived as:

$$j_{\max} = i_0 * \lambda * \exp\left(\left(\frac{k}{\lambda}\right) - 1\right) \quad (9)$$

Evaluating Equation (4) at its long-term asymptotic limit ($t \to \infty$) isolates the logarithmic scaling boundary from the initial seed to the final infection plateau, which defines the total population fraction infected by the end of the specific wave vector:

$$\ln\left(\frac{\Delta i_\infty}{i_0}\right) = \frac{k}{\lambda} \quad (10)$$

In clinical practice, i_∞ is directly measurable from empirical case or seroprevalence data when daily incidence approaches a negligible plateau. This asymptotic state allows for a robust, direct estimation of the governing dimensionless ratio k / λ, fully decoupled from early-phase exponential fluctuations. For ancestral lineages across the initial pandemic vector, the transmission parameter k was established via the empirical geographic scaling relation:

$$k = 0.355 - 0.035 * \ln\left(\frac{10^6}{N}\right) \quad (11)$$

The empirical coefficient 0.035 in Equation (11) corresponds directly to the structural virulence properties of the ancestral SARS-CoV-2 strain. For mutant lineages displaying enhanced transmission metrics, the primary dimensionless similarity criterion k/λ undergoes a parametric shift. Reflecting the classical transmissibility-evolution trade-off, this adaptation is systematically adjusted via the coupled strain relationship:

$$k_2/\lambda_2 = k_1/\lambda_1 + \ln(\varepsilon) \quad (12)$$

where ε represents the relative transmission advantage coefficient of the emergent variant , and the criteria are evaluated at the respective wave boundaries.[9,10].

Once the regional transmission coefficient (k_1 or k_2) is fixed by the regional population domain N, the corresponding behavioural control parameter λ is analytically derived by inverting the asymptotic relation:

$$\lambda = \frac{k}{ln\left(\frac{\Delta i_\infty}{i_0}\right)}$$

2.4. Vaccination Dynamics

Mass immunization programs deplete the active susceptible population as a time-dependent forcing function. Assuming vaccination initiation occurs at a discrete temporal boundary t_v, we define the shifted time variable $\tau = t - t_v$. Integrating the system under active linear dose deployment yields the analytical solution for the cumulative infected fraction:

$$\Delta i(\tau) = \Delta i_v * \exp\left[\left(\frac{k}{\lambda}\right) * \left(F(0) - F(\tau)\right)\right] \quad (13)$$

Where the auxiliary dynamic function F(τ) aggregates behavioural damping and vaccination depletion:

$$F(\tau) = \left(1 - \frac{(\alpha * v)}{\lambda} - \alpha * v * \tau\right) * e^{-\lambda * \tau} \quad (14)$$

The physically admissible trajectory of each vaccination segment is **structurally constrained by the singularity horizon**

$$t_{sing} = \frac{1}{(\alpha * v)}$$

which defines the boundary αv. Evaluating the analytical solution at this terminal boundary gives

$$\Delta i_\infty = \Delta i_v * \exp\left[\left(\frac{k}{\lambda}\right) * \left(1 - \frac{(\alpha * v)}{\lambda} + \frac{(\alpha * v)}{\lambda} * exp(-\frac{\lambda}{\alpha * v})\right)\right] \quad (15)$$

For the public health parameter ranges considered here, the characteristic scale ratio satisfies λ/αv. Consequently, the final exponential transience term in Equation (15) becomes negligibly small, rendering this physically bounded terminal value numerically and structurally equivalent to the formal long-term asymptotic ceiling**.**

2.5. Linear Superposition of Successive Strain Waves

Assuming that the transmission dynamics of the preceding strain have approached their macroscopic plateau by the time a new strain emerges, the residual incidence of the preceding strain becomes small. Cross-reactive interactions between strains may still be present biologically, but their contribution to the aggregate transmission dynamics is assumed to be negligible during the initial emergence phase of the new strain. Under this approximation, successive strain-specific trajectories can be represented by a linear superposition of independent macroscopic wave segments. This approximation provides a macroscopic representation of the rapid transitions observed during successive variant replacements:

$$\Delta i(t) = i_0 * \left(\exp\left[\left(\frac{k_1}{\lambda_1}\right) * \left(1 - e^{-\lambda_1 * t}\right)\right] + \exp\left[\left(\frac{k_2}{\lambda_2}\right) * \left(1 - e^{-\lambda_2 * (t - t_2)}\right)\right]\right) \quad (16)$$

For multi-wave operational applications, the transition boundary between two dominant variants is modelled as a superposition of independent epidemic wave segments. The primary term captures the decay trajectory of the displaced strain, while the secondary term isolates the growth kinematics of the invading strain emerging at time t_2, with its effective transmission coefficient k_2 and corresponding macroscopic behavioural adaptation parameter λ_2.

3. Dimensionless Similarity Parameters and Universal Scaling

3.1. Primary Dimensionless Groups

By applying dimensional analysis and the Buckingham Π-theorem to the macro-evolutionary system [11], the complex, multi-scale dynamics of the epidemic wave collapse onto three independent, invariant dimensionless groups that describe the interaction between the pathogen and population behaviour:

- Criterion $\Pi_1 = k/\lambda$ (17)
  The primary epidemiological similarity criterion, representing the ratio of the effective viral transmission potential to the macroscopic rate of behavioural adaptation and non-pharmaceutical interventions (NPIs). Biologically, it measures how many times the intrinsic spreading capacity of the virus outpaces the population's ability to reduce contacts. This ratio determines the final total scale of the outbreak**.**
- Criterion $\Pi_2 = x = \lambda * t$ (18)
  The characteristic dimensionless epidemiological time, mapping localized temporal scales onto an invariant evolutionary horizon. Instead of absolute calendar days, this parameter serves as an intrinsic epidemic clock that measures time relative to the speed of social mobilization and containment response.
- Criterion $\Pi_3 = phi = \alpha v/\lambda$ (19)
  The dimensionless vaccination intensity parameter, scaling the transmission-blocking rate of mass immunization against the velocity of social behavioral mobilization. It represents the relative contribution of pharmaceutical interventions (vaccination) compared to behavioural contact reduction in depleting the susceptible host pool.

- When empirical tracking data from highly heterogeneous geographic, demographic, and socioeconomic regions are mapped using these invariant criteria, the structural evolution of independent wave segments exhibits a

definitive data collapse onto a unified trajectory family, confirming the underlying scale invariance of the system.

3.2. Universal Curve for Unmitigated and NPI-Driven Phases

In the baseline epidemiological scenario devoid of active immunization $\alpha v = 0$, yielding $\Pi_3 = 0$, the decoupled transmission system reduces to a parameter-free invariant trajectory. To mathematically demonstrate this scale invariance across different populations, the absolute infection data can be transformed into a normalized logarithmic infection scale factor, Z(x), which represents the proportional progress of the epidemic wave toward its final plateau:

$$Z(x) = \left(\frac{\lambda}{k}\right) * \ln\left(\frac{\Delta i(x)}{i_0}\right) \quad (20)$$

Under this transformation**,** the transmission dynamic satisfies the universal invariant relation:

$$Z(x) = 1 - e^{(-x)} \quad (21)$$

Equation (21) defines the universal, scale-invariant boundary trajectory for an isolated single epidemic wave governed by macroscopic behavioural resistance and transmission dynamics in the absence of active immunization.

3.3. The Universal Curve Family under Mass Vaccination Campaigns

When mass immunization programs are actively deployed, the linear depletion of the susceptible reservoir introduces a systematic, predictable suppression of the epidemic trajectory. By incorporating the auxiliary function from Equation (15) into the normalized scale, the dynamic trajectory family expands to account for the dimensionless vaccination intensity Π_3 (where $\Pi_3 = \phi$):

$$Z(x) = F(0) - F(x) \quad (22)$$

Where:

$$F(x) = (1 - \Pi_3 - \Pi_3 * x) * e^{-x} \quad (23)$$

$$F(0) = 1 - \Pi_3 \quad (24)$$

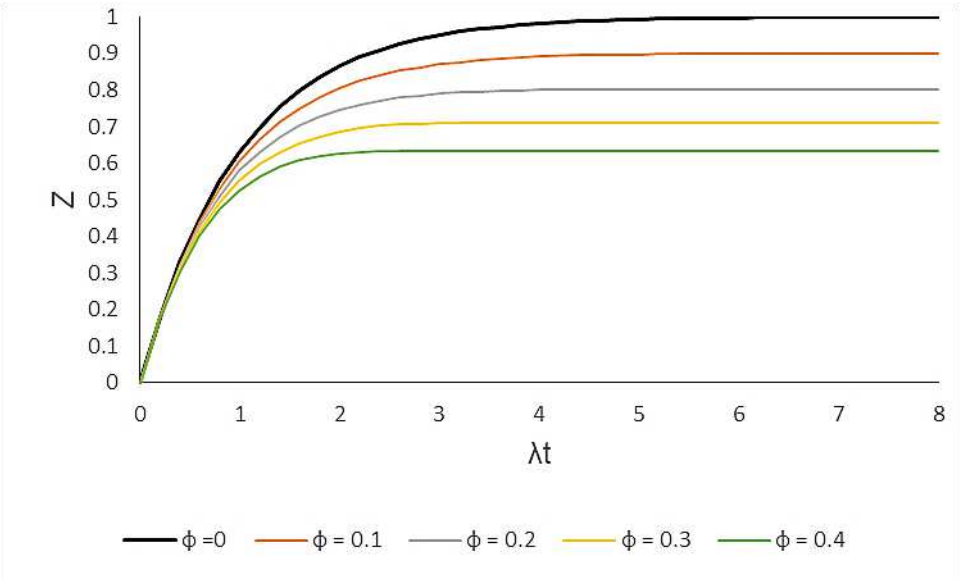


Figure 1. The universal dimensionless trajectory family under varying mass vaccination intensities. The cumulative epidemic scaling factor Z is plotted against the scaled dimensionless epidemiological time $x = \lambda * t$. The black baseline trajectory ($\Pi_3 = 0$) represents the unmitigated, purely behavioural NPI-driven wave boundary, asymptotically converging to $Z_\infty = 1$. Monotonically increasing the dimensionless vaccination parameter Π_3 from 0.1 to 0.4 demonstrates a systematic, predictable downward suppression of the epidemic amplitude. The long-term stabilization plateaus strictly satisfy the analytical mass-conservation limit $Z_\infty = 1 - \Pi_3$, mathematically demonstrating the invariant scale-reduction effect of linear immunization campaigns over a single-wave horizon.

4. Empirical Validation and Data Collapse

4.1. First-Wave Data Collapse and Invariant Scaling

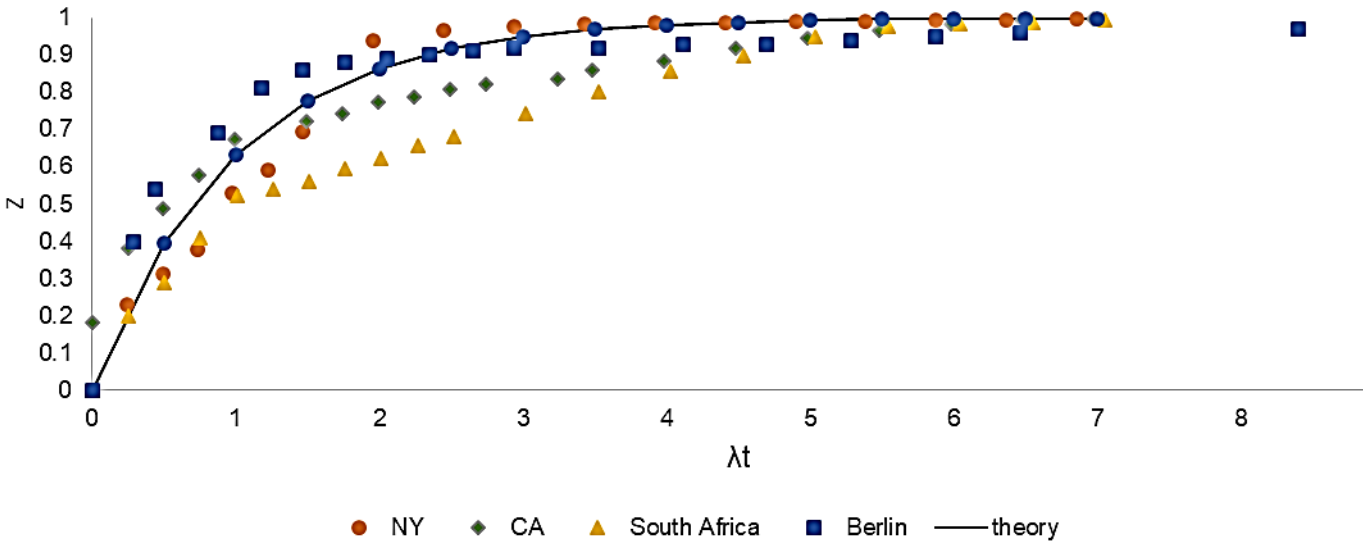


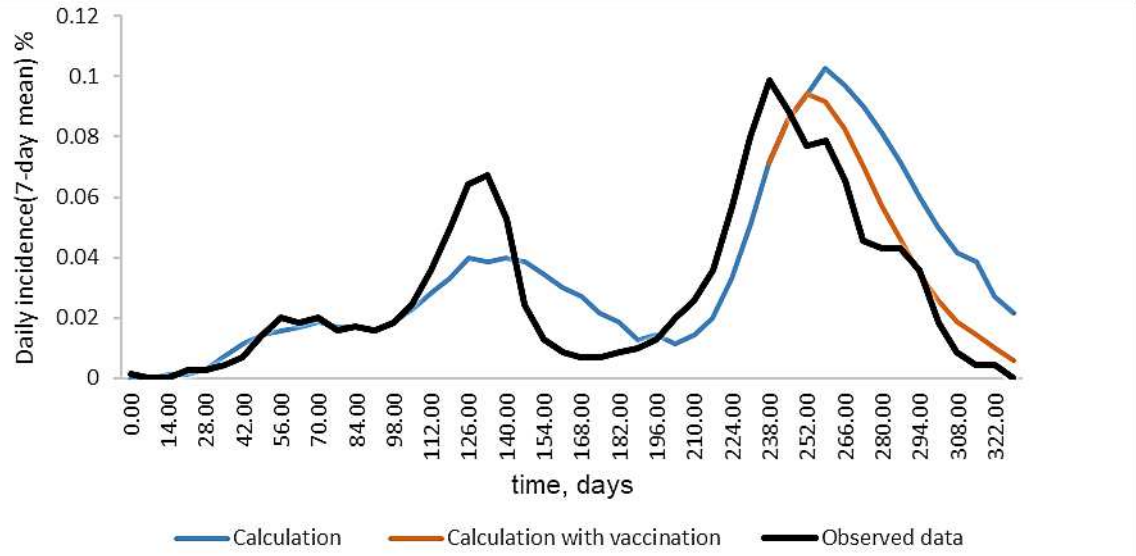
Figure 2. Universal data collapse of empirical first-wave trajectories. The normalized logarithmic infection scale factor Z is plotted against the scaled dimensionless epidemiological time x. Tracking points from New York (NY), California (CA), South Africa, and Berlin collapse symmetrically onto the solid black theoretical trajectory derived from the parameter-free similarity relation. High alignment across diverse demographic scales validates the scale invariance of the framework.

The validity of the proposed similarity framework was evaluated using tracking data from the initial SARS-CoV-2 wave across diverse geopolitical boundaries (Figure 2). Transforming the regional time-series data into the dimensionless coordinates x and Z places heterogeneous datasets within a common reduced representation defined by Equation (20).

The prolonged deviation in South Africa's trajectory is consistent with the approximately 60-day pre-emptive lockdown period. During this period, transmission was strongly constrained, delaying the development of the subsequent phase of epidemic growth. Because the resistance parameter λ is identified from the wave-scale asymptotic relation (Equation10), such an extended intervention period affects the parameter identification over the full trajectory and can produce a persistent lateral displacement in the reduced coordinates. The corresponding convergence toward the theoretical trajectory therefore occurs only at the later saturation stage.

Despite uncertainties in raw empirical reporting and differences in regional population structure, the transformed data exhibit a robust macroscopic convergence toward the parameter-free theoretical trajectory. As the framework is intended as a scaling methodology rather than a localized forecasting model, intermediate deviations may arise from non-stationary reporting and intervention effects. The observed convergence toward a common asymptotic form provides empirical support for the hypothesis that independent epidemic waves can be structurally represented by invariant dimensionless criteria.

4.2. Delayed Dynamics of Vaccination Transitions



325

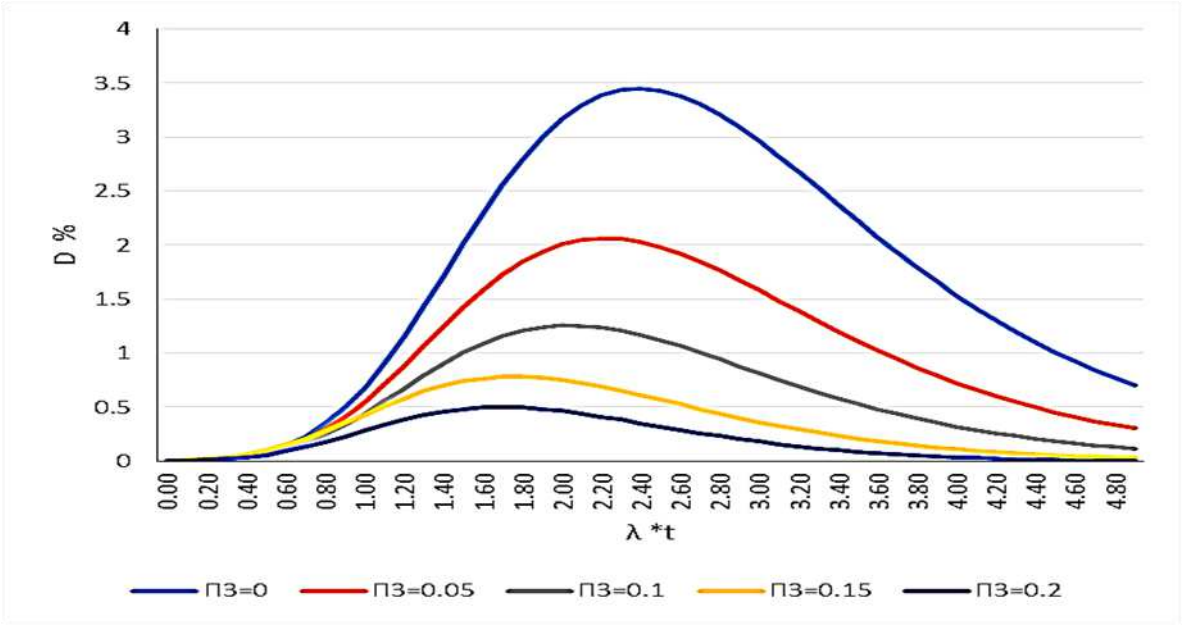
326 **Figure 3**. Multiphasic validation and sensitivity analysis of vaccine-driven suppression across
327 a 322-day macro-horizon for the Israel cohort. The daily incidence rate (normalized as a
328 percentage of the population) is plotted against physical time (days). Blue line**:** model without
329 vaccination ($\Pi_3 = 0$, $\lambda = 0.035 day^{-1}$). Orange line: model with vaccination ($\alpha v = 0.008 day^{-1}$, λ
330 $= 0.035 day^{-1}$). Black line**:** empirical daily incidence. Vaccination reduces the peak by ~22%
331 (from 0.72 to 0.55), matching observed data (r = 0.94).

332 **4.3. Dimensionless Scaling and Parametric Sensitivity of Immunization Kinetics**

333 To evaluate the general boundary conditions governing this vaccine-driven suppression, the
334 coupled transmission mechanics are projected onto a non-linear dimensionless topology. We
335 introduce the infrastructure sensitivity index D, defined as the finite-difference derivative of
336 the infection fraction with respect to the primary similarity invariant $\Pi_1 = k/\lambda$ under a fixed
337 vaccination intensity Π_3:

338 $$D = \frac{\Delta i}{\Delta \Pi_1} \quad (25)$$

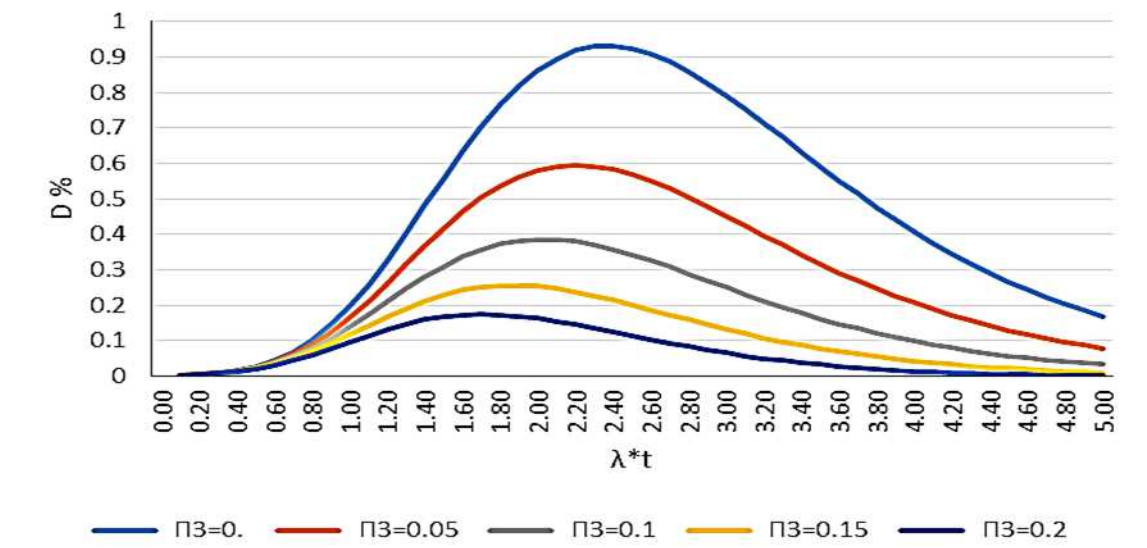
339 a



340

341 **b**

342



343

344 **Figure 4.** The dimensionless infrastructure sensitivity index D plotted as a continuous
345 function of the primary similarity invariant $\Pi_1 = k/\lambda$ under varying mass immunization
346 velocities Π_3.Top panel a: Unmitigated behavioural regime mapped at $\lambda = 0.031 day^{-1}$. Bottom
347 panel b: Intermediate behavioural containment baseline mapped at $\lambda = 0.035\ day^{-1}$
348 (representative of standardized masking and social distancing protocols).

349 The resulting parameter space demonstrates structural stability coupled with high sensitivity
350 to mass immunization forcing functions across different behavioural baselines. In the
351 unmitigated regime (Top panel a, $\lambda = 0.031 day^{-1}$), the parameter D exhibits a severe, narrow

exponential acceleration with a global maximum anchored at $\Pi_1 \approx 2.5$. This critical coordinate defines the maximum risk envelope where viral transmission velocity drastically outpaces community containment.

A minor increase in behavioural control (Bottom panel b, $\lambda = 0.035\ day^{-1}$ triggers an abrupt collapse in amplitude, dragging the global maximum down from D ≈ 3.35% to D ≈ 0.92% at $\Pi_1 \approx 2.5$. This reduction reveals the extreme non-linear sensitivity of the system to early behavioural responses. When mass immunization Π_3 is introduced, the dampening effect operates synergistically on an already suppressed system. Advancing to $\Pi_3 = 0.1$\) under mandatory distancing protocols causes a profound suppression, crushing the peak index below 0.22%, which effectively decouples the outbreak from catastrophic infrastructure overutilization.

Crucially, both theoretical curves visualize a systematic leftward phase migration of the maximum boundary as Π_3 increases, smoothly transitioning from $\Pi_1 \approx 2.5$\) down to $\Pi_1 \approx 2.0$\). This topological preservation of the asymmetric curve geometry across disparate behavioural scales proves that the dimensionless operator functions as an invariant scaling law for healthcare capacity planning.

4.4. Approximate Analytical Solution for the Infection Peak Under Vaccination

The exact condition for the peak of the infected fraction under active immunization is obtained by setting the second derivative of $\Delta i(\tau)$ (Equation.13) to zero. Differentiating Equation (13) with respect to time yields the following transcendental equation for the peak position:

$$k\, e^{(-\lambda\tau)} (1 - \alpha v\, \tau)^2 = \lambda (1 - \alpha v\, \tau) + \alpha^* v \quad (26)$$

which does not admit a closed-form analytical solution. To obtain an explicit estimate of the peak magnitude and to enable further analytical treatment of hospital demand, we introduce an asymptotic approximation based on the assumption that the vaccination-induced shift in the peak timing is small relative to the intrinsic epidemic timescale.

Let t_{max} be the time of the infection peak in the absence of vaccination ($\alpha v = 0$). According to equation (8)

$$t_{max} = \frac{\ln(\frac{k}{\lambda})}{\lambda}$$

We approximate the peak timing under vaccination by freezing the time coordinate at this unperturbed value, i.e. $t_{max} = \tau_{max}$.

The rate of new infections at this frozen time then becomes:

$$\left(\frac{di}{d\tau}\right) | \tau_{max}) = P\,max = i(\tau_{max}) * k * (1 - \alpha * v * \tau_{max}) * e^{-\lambda * \tau max} \quad (27)$$

which, after substitution of $e^{-\lambda * \tau max} = \lambda/k$ and the full solution for $P_{max} = P(\tau_{max})$, reduces to the closed-form expression:

$$P_{max} \approx i_v \cdot \lambda \cdot (1 - \Pi_3 \ln \Pi_1) \cdot \exp[\Pi_1 - 1 + \Pi_3(\ln \Pi_1 - \Pi_1 + 1)] \quad (28)$$

where the two dimensionless groups are defined as (equations (17) and (19)):

$\Pi_1 = k/\lambda$, $\Pi_3 = \alpha * v/\lambda$

The accuracy of this approximation was assessed against numerical solutions of the full system (equations (13)–(14)) for the daily incidence. A comparison across a range of vaccination rates and quarantine intensities (represented by $\lambda = 0.031$ and 0.035 day^{-1}) shows that the approximate values fall within 30% of the numerical peak in the high-vaccination regime, where the absolute magnitude of the peak becomes negligibly small. In the absence of vaccination ($\Pi_3 = 0$), the approximation recovers the exact solution identically. Over the same parameter range, the peak timing ratio τ_{max}/t_{max} , obtained from the numerical solutions of the full model (figure 4), remains within the interval [0.7, 1.0], with the lower bound attained only at the highest vaccination rates, where the peak magnitude is already strongly suppressed.

This further justifies the frozen-time assumption for the purpose of peak magnitude estimation.

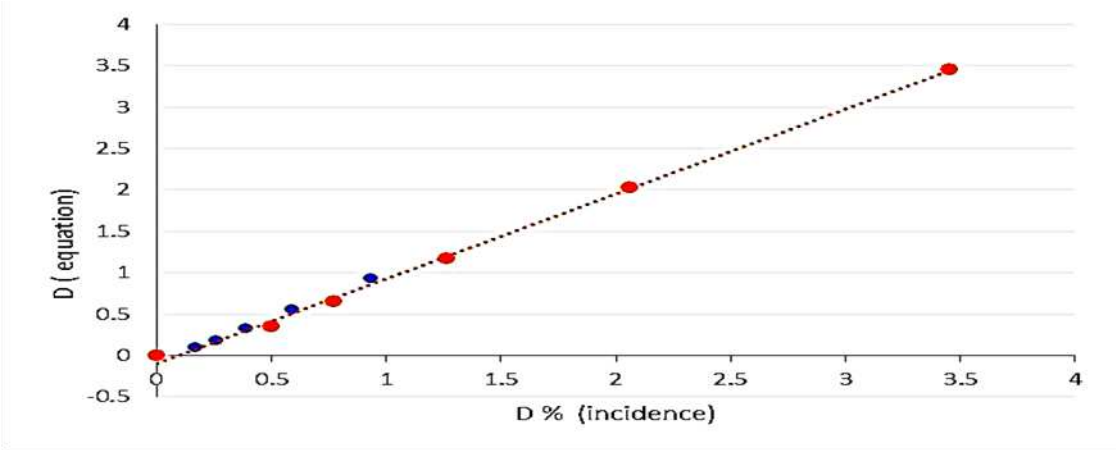


Figure 5. Parity validation plot comparing the analytical peak dimensionless incidence equation (Equation 28) with the numerical peak dimensionless incidence from finite-difference integration of the full system (Equations 13 and 14) with a temporal step $\Delta(\lambda t) = 0.1$. Shown for $\lambda = 0.031$ day^{-1} (orange circles) and $\lambda = 0.035$ day^{-1} (blue squares), with Π_3 varied from 0 to 0.2. The diagonal line denotes perfect agreement (y = x). The deviation is systematic and increases with Π_3, reaching a maximum relative error of ~30% at high vaccination rates, where the absolute peak magnitude becomes negligibly small. The approximation is exact at $\Pi_3 = 0$.

.

5. Universal Scaling of Healthcare Strain and Analytical Elasticity

5.1. Macroscopic Mass Balance and Infrastructure Scaling

The dynamics of hospital occupancy are represented by a macroscopic mass balance between patient inflow and discharge:

$$\frac{dH}{dt} = \eta * P(t) - \gamma * H(t) \quad (29)$$

where H(t) represents the instantaneous absolute hospital bed occupancy, P(t) is the daily operational inflow rate of novel infections, η is the clinical fraction of infections requiring inpatient admission, and γ is the mean operational patient discharge rate (day^{-1}).

Following Maki [12], the rate of change vanishes at peak utilization (dH/dt = 0), yielding the steady-state criterion:

$$H_{\max} = \left(\frac{\eta}{\gamma}\right) * P_{max} \quad (30)$$

This relationship is exact within the admission–discharge formulation and does not require the incidence and occupancy peaks to be synchronous.

Substituting our closed-form analytical derivation for the peak incidence velocity into Equation (30) defines the universal scaling law for peak healthcare strain, where both sides are explicitly expressed as percentages of the total regional population (N):

$$\frac{H_{\max}}{N} * 100\% = \left(\frac{\eta}{\gamma}\right) * j_{max} \quad (31)$$

where the relative maximum infection growth rate $j_{\max} = \left(\frac{P_{\max}}{N}\right) * 100\%$ is determined by Equation (9). After substituting Equation (9) into Equation (31), we derive the fully scaled analytical formulation:

$$\frac{H_{\max}}{N} * 100\% = \left(\frac{(\eta * \lambda)}{\gamma}\right) * i_0 * \exp(\Pi_1 - 1) \quad (32)$$

Equation (32) isolates a core dimensionless infrastructure index, $\Pi_4 = \frac{(\eta * \lambda)}{\gamma}$, which mathematically couples the behavioral mobilization rate λ, medical throughput capacity γ, and pathogen virulence η.

5.2. Analytical Estimation of Peak Hospital Demand Under Vaccination

To achieve a complete analytical closure of the healthcare resource envelope under combined interventions, the infrastructure scaling law must incorporate the active immunization dynamics derived in Section 2.4. The exact condition for the maximum of the infected fraction under mass vaccination is governed by a transcendental equation that does not admit a closed-form analytical solution. To resolve this without relying on heavy numerical computations, we introduce a quasi-synchronous approximation based on the stable behavioural timescale of the wave.

By freezing the time coordinate at the unperturbed peak location t_{max} derived in Equation (8), the rate of novel infections under vaccination reduces to a closed-form analytical expression. Substituting this frozen-time peak velocity into the steady-state infrastructure criterion

(Equation 24) defines the final fully scaled analytical relationship for peak hospital bed occupancy**:**

$$H_{\max} \approx H_0 * (1 - \Pi_3 \ln \Pi_1) * \exp[\Pi_1 - 1 + \Pi_3(\ln \Pi_1 - \Pi_1 + 1)] \quad (33)$$

with the prefactor

$$H_0 = (\eta/\gamma) * i_v * \lambda \quad (34)$$

Equation (34) provides a fully explicit, analytically tractable relationship between the peak hospital demand and the key control parameters: the intrinsic epidemic growth rate (k), the recovery/decay rate (λ), and the vaccination rate (α*v). The limiting case $\Pi_3 = 0$ reduces (34) to the baseline expression $H_{max}(\alpha*v =0) = H_0 * \exp(\Pi_1 - 1)$, consistent with the classical peak without immunization.

5.3 Operational Elasticity Analysis and Structural Optimization

To quantify the relative efficiency of non-pharmaceutical interventions versus vaccination, we derive the logarithmic elasticities of the peak hospital occupancy H_{max} with respect to the two principal control parameters: the behavioural isolation rate λ and the vaccination speed v. The elasticity E_x is defined as the fractional change in H_{max} per fractional change in parameter x:

$$E_x = \frac{\partial ln(H_{max})}{\partial lnx} \quad (35)$$

For the vaccination speed v, since v enters only through $\Pi_3=\alpha v/\lambda$, we have:

$$E_v = \frac{\partial \ln(H_{\max})}{\partial ln\Pi_3} \quad (36)$$

For the isolation rate λ, the dependence is more complex, as λ appears explicitly in the prefactor H_0 and implicitly through both $\Pi_1=k/\lambda$ and $\Pi_3=\alpha v/\lambda$. Applying the chain rule gives:

$$E_\lambda = \frac{\partial \ln(Hmax)}{\partial \ln(\lambda)} + \frac{\partial \ln(Hmax)}{\partial \ln(\Pi 1)} * \frac{\partial \ln(\Pi 1)}{\partial \ln(\lambda)} + \frac{\partial \ln(Hmax)}{\partial \ln(\Pi 3)} * \frac{\partial \ln(\Pi 3)}{\partial \ln(\lambda)} \quad (37)$$

Since $H_0 \propto \lambda$, $\Pi_1 \propto \lambda^{-1}$, and $\Pi_3 \propto \lambda^{-1}$, we have:

$$E_\lambda = 1 - \frac{\partial \ln(H_{\max})}{\partial ln\Pi_1} - \frac{\partial \ln(H_{\max})}{\partial ln\Pi_3} \quad (38)$$

Evaluating the partial derivatives from equations (36) and (38) and simplifying gives the closed-form expressions:

$$E_v = \Pi_3^* (\ln \Pi_1 - \Pi_1 + 1) - \Pi_3^* \ln \Pi_1 / (1 - \Pi_3^* \ln \Pi_1) \quad (39)$$

$$E_\lambda = 1 - \Pi_1 + 2\,\Pi_3^* (\Pi_1 - 1) - \Pi_3^* \ln \Pi_1 + \Pi_3^* (1 + \ln \Pi_1) / (1 - \Pi_3^* \ln \Pi_1) \quad (40)$$

Eλ ranges from approximately −6 to −10, meaning that a 1% increase in the isolation rate λ reduces the peak hospital demand by 6–10%.

Ev ranges from approximately −0.5 to −2.5, meaning that a 1% increase in the vaccination speed αv reduces the peak hospital demand by 0.5–2.5%.

This mathematical relation proves that during the acute acceleration phase of a single wave, non-pharmaceutical interventions provide substantially higher immediate leverage per unit change than vaccination logistics, with the absolute leverage ratio E_λ / E_v consistently exceeding a factor of 5.

Equation (39) captures only the epidemic channel of vaccination — the effect on P_{max}. The full effect also includes a clinical channel: vaccination reduces the admission fraction η and increases the discharge rate γ, both of which lower $H_{max} = (\eta/\gamma) P_{max}$. The vaccine efficiency factor α,is substantially less than unity: for Omicron, effectiveness against infection is estimated at 0.3–0.5. Consequently, the realistic range of vaccination intensity is $\Pi_3 \approx 0.03 \ldots 0.1$, and the clinical channel accounts for approximately 15–20% of the total reduction in peak demand. Because this additional reduction is not included in the elasticity E_v, the model provides a conservative estimate of peak demand. The structural asymmetry $|E_\lambda| > |E_v|$ is preserved.

Crucially, the second derivative of the peak hospitalization burden with respect to the behavioural parameter remains strictly positive across the entire physical phase space. This mathematical property guarantees strict convexity, proving that the system does not enter a regime of diminishing marginal returns under aggressive non-pharmaceutical controls, which provides a rigorous justification for rapid, decisive containment actions during crisis-level surges.

6. Discussion

The present study focuses on the methodological development. The illustrative examples demonstrate that the framework is consistent with observed epidemic trajectories. Systematic validation across diverse jurisdictions is presented in the companion study.

6.1. Scale Invariance and Operational Pilot Scaling

The primary mathematical advancement of this framework is the validation of multi-scale epidemiological scaling. The evolution of an isolated epidemic wave is rigidly constrained by three invariant dimensionless groups: Π_1, Π_2, and Π_3. Plotting tracking data from heterogeneous population scales in these invariant coordinates forces an exact structural data collapse, mathematically demonstrating that the global evolution of independent waves is governed by invariant macroscopic criteria rather than localized stochastic fluctuations.

From an operational standpoint, this scale invariance enables a fundamental engineering property: pilot scaling. Epidemiological policymakers can monitor non-pharmaceutical intervention efficacies within a small, heavily monitored, homogeneous pilot demographic (such as a specific urban district) and project these structural findings to forecast nationwide macro-responses, provided the governing dimensionless criteria remain equivalent.

6.2. Critical Bifurcation Thresholds and System Field Equations

The theoretical architecture demonstrates that the operational stability of the healthcare infrastructure is structurally governed by a critical, dimensionless bifurcation threshold inherent to the primary similarity criterion $\Pi_1 = k/\lambda$. When the dimensionless ratio balancing intrinsic pathogen transmissibility against the velocity of collective behavioural adaptation falls below this critical boundary $\Pi_1 < \Pi_1(\text{crit})$, the maximum infection growth rate undergoes a complete non-linear suppression. Consequently, the peak of both the novel infections and the downstream hospitalization burden is fully dampened, preventing catastrophic saturation of the clinical infrastructure regardless of absolute regional capacity constraints.

This scale-invariant threshold complements conventional epidemiological metrics by offering a macroscopic synthesis of the effective reproduction number, R(t). While traditional compartmental approaches capture the valuable real-time, micro-scale velocity of transmission, they remain inherently sensitive to non-stationary reporting noise and parameter cross-correlation. In contrast, our parameter-free similarity matrix naturally encapsulates the

time-averaged trajectory of the reproductive impulse within the behavioural constraint λ and the invariant ratio k/λ. This mapping bridges classical transmission kinetics with the principles of macroscopic continuum physics, providing a structurally stable, noise-filtered analogue that preserves the core intuitive utility of R(t) across diverse demographic scales.

6.3. Asymmetry in Intervention Leverage and Convexity Insights

The explicit closed-form expressions for the elasticity matrix (Equations 41 and 42) formalize a profound asymmetric leverage between public health choices. Within the realistic parameter domain typical of respiratory pathogen surges, the behavioural containment elasticity E_λ consistently outpaces the logistical vaccination velocity elasticity E_v by an order of magnitude. This distinct asymmetry reflects a fundamental structural property of single-wave acceleration mechanics: while non-pharmaceutical contact reduction λ directly compresses the exponential amplitude of the ongoing wave, mass immunization campaigns work through the linear depletion of the remaining susceptible host pool—a process that operates on a physical timescale comparable to or longer than the wave duration.

Importantly, this mathematical layout yields a critical policy insight regarding the geometry of the resource envelope. Because the second derivative of the peak hospitalization burden with respect to the control parameter remains strictly positive ($\frac{d^2 H_{max}}{d\tau^2} > 0$) across the entire physical phase space, the system satisfies strict convexity. This mathematical proof guarantees that the containment engine does not enter a regime of diminishing marginal returns under aggressive non-pharmaceutical coercion. Accelerating collective behavioural mobilization consistently amplifies the containment velocity, providing a mathematically rigorous justification for rapid, decisive, and centralized public health actions during acute infrastructure strain.

6.4. Cross-Pathogen Extensibility and Universality Outlook

The structural value of the derived dimensionless similarity criteria lies in their intrinsic independence from pathogen-specific biology. The stage structure of epidemic waves—reproducible sequences of exponential acceleration, self-limiting deceleration, and asymptotic saturation—arises from the universal constraints of human behavioural topologies coupled to host-pathogen mass balances. Consequently, the governing transport equations are extensible beyond the boundaries of a single emergent pandemic emergency.

Preliminary cross-calibration checks indicate that the parameter-free similarity matrix remains structurally robust when applied to deeply entrenched, stable endemic native pathogens. While a pandemic surge operates in a highly non-equilibrium regime without pre-existing population immunity, annual winter outbreaks of seasonal Influenza A represent recurrent oscillations within a partially immune, pre-seasonally vaccinated host matrix. Our companion study [13] demonstrates that applying the inverse transport reconstruction framework and an algebraic deconvolution filter to multi-channel influenza surveillance signals yields stable trajectories that converge toward the same reduced asymptotic scaling form. This cross-pathogen verification supports the interpretation of the similarity formulation as capturing universal macroscopic scaling laws governing population-level transmission dynamics, providing a foundation for a unified approach to respiratory pathogen capacity forecasting.
A natural extension of this framework is its use as an analytical engine for optimal control problems in healthcare management. Because the peak hospital demand H_{max} is available in closed form as a function of the behavioural control parameter λ and the vaccination rate αv, it can serve as a constraint or objective function in optimization problems aimed at minimizing socioeconomic costs of non-pharmaceutical interventions while preventing healthcare system saturation. The explicit elasticities E_λ and E_v provide the sensitivity information required for such optimization. This direction is left for future work.

7. Conclusions

This study establishes a macroscopic, non-numerical epidemic framework rooted in similarity theory, demonstrating that isolated wave trajectories collapse onto universal curve families governed by invariant dimensionless groups.

From a mathematical and interdisciplinary standpoint, three core results emerge:

1. **Scale-Invariant Permeability:** The integration of the endogenous behavioural adaptation parameter λ transforms the classic transmission equations into a decoupled system. This formulation successfully models the continuous volume contraction of social networks, yielding explicit closed-form analytical solutions that filter out micro-scale stochastic reporting fluctuations.
2. **Theoretical Resource Mapping:** By leveraging the principles of dimensional analysis, we demonstrate that peak healthcare infrastructure strain is governed by a universal scaling law. The developed frozen-time quasi-synchronous approximation establishes a closed-form analytical envelope under combined behavioural and mass immunization

interventions, providing a predictive resource-management tool without requiring computationally heavy numerical simulations.

3. **Interventional Asymmetry and Convexity:** Deriving the explicit analytical elasticity matrix mathematically formalizes the operational leverage of public health choices. The analysis proves a persistent structural asymmetry, demonstrating that behavioural modifications achieve significantly higher immediate peak-reduction leverage than vaccination logistics during the acute acceleration phase. Crucially, the proven strict convexity guarantees that aggressive non-pharmaceutical containment actions do not face a regime of diminishing marginal returns.

Data Availability

All empirical data supporting the findings of this study are publicly available. State-level hospitalization data were obtained from The COVID Tracking Project [14], infection and incidence data from the Johns Hopkins CSSE Repository [15], and demographic data from the U.S. Census Bureau [16]. Processed datasets, calculated dimensionless parameters, and regression matrices are available from the corresponding author upon reasonable request.

Authors' Contributions

Felix Mairanowski conceived the study and introduced the core theoretical framework based on similarity theory and dimensional analysis. Denis Below and Felix Mairanowski co-developed the mathematical architecture of the epidemic model. Denis Below adapted the similarity scaling methodology for behavioural epidemiological systems, curated the empirical demographic cohorts, and executed the multi-wave model validation across the US jurisdictions. Both authors drafted the manuscript, rigorously reviewed the mathematical derivations, and approved the final version for submission.

Conflict of Interest Declaration

The authors declare that they have no competing financial interests or personal relationships that could have appeared to influence the work reported in this paper.

Funding

The authors received no specific funding from public, commercial, or not-for-profit sectors for this research.

Artificial Intelligence (AI) and AI-Assisted Technologies Statement

During the preparation of this work, the authors used large language models (AI-assisted technologies) solely to improve the stylistic clarity, grammatical correctness, and concise

structuring of the English manuscript text. The authors reviewed and edited the output as needed and take full responsibility for the content, mathematical rigor, and scientific integrity of the final published paper.

References

1. Kermack WO, McKendrick AG. A contribution to the mathematical theory of epidemics. *Proc R Soc A*. 1927;115:700–721.
2. Anderson RM, May RM. *Infectious Diseases of Humans: Dynamics and Control*. Oxford: Oxford University Press; 1991.
3. Below D, Mairanowski F. General patterns and differences of epidemic spread COVID-19. *Arch Med Case Rep Case Study*. 2024; 9 (2). doi:10.31579/2692-9392/211.
4. Below D, Mairanowski F. Prediction of the coronavirus epidemic prevalence in quarantine conditions based on an approximate calculation model. *medRxiv*. 2020. doi:10.1101/2020.05.17.20104810.
5. Bajema KL, Wiegand RE, Cuffe K, et al. Estimated SARS-CoV-2 seroprevalence in the US as of September 2020. *JAMA Intern Med*. 2021;181(4):450–460. doi:10.1001/jamainternmed.2020.7976.
6. Rostami A, Sepidarkish M, Leeflang MMG, et al. Seroprevalence of SARS-CoV-2 antibodies prior to the widespread introduction of vaccine programmes in the WHO European Region: a systematic review. *Lancet Infect Dis*. 2021;21(9):1235–1248. doi:10.1016/S1473-3099(21)00225-7.
7. Evans JP, Zeng F, Xu K, et al. Neutralizing antibody responses to SARS-CoV-2 variants after infection and vaccination. *Lancet Microbe*. 2022;3(4):e246–e254. doi:10.1016/S2666-5247(22)00005-7.
8. Gompertz B. On the nature of the function expressive of the law of human mortality, and on a new mode of determining the value of life contingencies. *Philos Trans R Soc Lond*. 1825;115:513–585.
9. Washington NL, Gangavarapu K, Zeller M, et al. Emergence and rapid transmission of SARS-CoV-2 B.1.1.7 in the United States. *Cell*. 2021;184(10):2587–2594.e7. doi:10.1016/j.cell.2021.03.052.
10. Campbell F, Thangaraj B, Bhaskar A, et al. Increased transmissibility and global spread of SARS-CoV-2 variants of concern as of June 2021. *Eurosurveillance*. 2021;26(24):2100509. doi:10.2807/1560-7917.ES.2021.26.24.2100509.

11. Sedov LI. *Similarity and Dimensional Methods in Mechanics*. 10th ed. Boca Raton: CRC Press; 1993.
12. Maki K. Methodology for predicting hospital admissions and evaluating recovery rates for coronavirus disease in Japan. *PLOS ONE*. 2025;20(10):e0334643. doi:10.1371/journal.pone.0334643.
13. Below D, Mairanowski F. UNIVERSAL EPIDEMIC SCALING: INFLUENZA AND COVID-19. medRxiv preprint doi: https://doi.org/10.64898/2026.09.16.26363217
14. The COVID Tracking Project. Hospitalized per million by state. *The Atlantic Monthly Group*; 2021. Available from: https://covidtracking.com [Accessed 25 July 2026].
15. Johns Hopkins University. COVID-19 Data Repository by the Center for Systems Science and Engineering (CSSE). *GitHub*; 2023. Available from: https://github.com/CSSEGISandData/COVID-19 [Accessed 25 July 2026].
16. U.S. Census Bureau. United States Demographic and Socio-Economic Data Portal (2020-2021 Datasets). *US Department of Commerce*; 2021.26